Brain Imaging and Behavior (2019) 13:1–14
DOI 10.1007/s11682-017-9727-6

ORIGINAL RESEARCH

High-sensitivity neuroimaging biomarkers for the identification of amnestic mild cognitive impairment based on resting-state fMRI and a triple network model

Enyan Yu[1] · Zhengluan Liao[1] · Yunfei Tan[1] · Yaju Qiu[1] · Junpeng Zhu[1] · Zhang Han[2] · Jue Wang[3] · Xinwei Wang[1] · Hong Wang[1] · Yan Chen[1] · Qi Zhang[1] · Yumei Li[4] · Dewang Mao[4] · Zhongxiang Ding[4]

Published online: 3 May 2017

Abstract Many functional magnetic resonance imaging (fMRI) studies have indicated that Granger causality analysis (GCA) is a suitable method for revealing causal effects between brain regions. The purpose of the present study was to identify neuroimaging biomarkers with a high sensitivity to amnestic mild cognitive impairment (aMCI). The resting-state fMRI data of 30 patients with Alzheimer's disease (AD), 14 patients with aMCI, and 18 healthy controls (HC) were evaluated using GCA. This study focused on the "triple networks" concept, a recently proposed higher-order functioning-related brain network model that includes the default-mode network (DMN), salience network (SN), and executive control network (ECN). As expected, GCA techniques were able to reveal differences in connectivity in the three core networks among the three patient groups. The fMRI data were preprocessed using DPARSFA v2.3 and REST v1.8. Voxel-wise GCA was performed using the REST-GCA in the REST toolbox. The directed (excitatory and inhibitory) connectivity obtained from GCA could differentiate among the AD, aMCI and HC groups. This result suggests that analysing the directed connectivity of inter-hemisphere connections represents a sensitive method for revealing connectivity changes observed in patients with aMCI. Specifically, inhibitory within-DMN connectivity from the posterior cingulate cortex (PCC) to the hippocampal formation and from the thalamus to the PCC as well as excitatory within-SN connectivity from the dorsal anterior cingulate cortex (dACC) to the striatum, from the ECN to the DMN, and from the SN to the ECN demonstrated that changes in connectivity likely reflect compensatory effects in aMCI. These findings suggest that changes observed in the triple networks may be used as sensitive neuroimaging biomarkers for the early detection of aMCI.

Keywords Functional magnetic resonance imaging (fMRI) · Alzheimer's disease · Amnestic mild cognitive impairment · Granger causality analysis · Default-mode network

Abbreviations

ACC	Anterior cingulate cortex
AD	Alzheimer's disease
ALFF	Amplitude of low-frequency fluctuations
aMCI	Amnestic mild cognitive impairment
ANCOVA	One-way analysis of covariance
ANOVA	One-way analysis of variance
BOLD	Blood oxygenation level-dependent
dACC	Dorsal anterior cingulate cortex
dlPFC	Dorsolateral prefrontal cortex
DMN	Default-mode network
ECN	Executive control network
EPI	Echo-planar imaging
FC	Functional connectivity
fMRI	Functional magnetic resonance imaging

Electronic supplementary material The online version of this article (doi:10.1007/s11682-017-9727-6) contains supplementary material, which is available to authorized users.

✉ Zhongxiang Ding
hangzhoudzx73@126.com

[1] Department of Psychiatry, Zhejiang Provincial People's Hospital, Hangzhou 310014, China

[2] Center for Cognition and Brain Disorders, Hangzhou Normal University, Zhejiang, Hangzhou 311121, China

[3] Department of Psychiatry, Tongde Hospital of Zhejiang Province, Hangzhou 310012, China

[4] Department of Radiology, Zhejiang Provincial People's Hospital, 158, Shangtang Rd, Hangzhou 310014, China

FOV	Field of view
GCA	Granger causality analysis
HC	Healthy controls
IPC	Inferior parietal cortex
ITC	Inferior temporal cortex
MMSE	Mini mental state evaluation
MoCA	Montreal cognitive scale
MPFC	Medial prefrontal cortex
MPRAGE	Magnetization-prepared rapid gradient echo
PCC	Cingulate cortex
PCC	Posterior cingulate cortex
PPC	Lateral posterior parietal cortex
ROI	Region of interest
SN	Salience network
TE	Echo time
TR	Repetition time

Introduction

Alzheimer's disease (AD) is a progressive neurodegenerative disease that is clinically characterized by memory decline and other cognitive function impairments. These impairments can affect orientation, immediate memory, delayed memory, attention, calculation, language, abstraction, visuospatial abilities, and executive functions. Amnestic mild cognitive impairment (aMCI) refers to a level of memory decline and cognitive degeneration among ageing individuals who do not meet the criteria for dementia, and is considered the prodromal stage of dementia with a high risk of transition to AD (Morris et al. 2001). Petersen et al. (2005) showed that the short-term (6 to 12 months) use of donepezil for aMCI treatment results in a more marked decrease in AD progression than observed in controls, whereas no differences were observed at 36 months. This finding indicates that early intervention more effectively delays the progression of AD than late-stage treatment, and prolongs patient survival. Individuals with aMCI have a high risk of conversion to AD (Ganguli et al. 2011). Therefore, early identification of aMCI is particularly important.

In recent decades, resting-state fMRI (rs-fMRI) has been utilized for the early detection of aMCI. Many findings based on rs-fMRI analyses have revealed that changes in the amplitude of low-frequency fluctuations (ALFF) (Bai et al. 2008; Li et al. 2002), local functional connectivity as revealed by regional homogeneity (ReHo), and long-range functional connectivity (FC) (Binnewijzend et al. 2012; Sorg et al. 2007) can be detected in the prodromal stage of AD. These changes are concentrated in the parietal cortex, precuneus, posterior cingulate cortex (PCC), anterior cingulate cortex (ACC), medial prefrontal cortex (MPFC), hippocampus, and thalamus (Andreasen and Redrobe 2009; De Luca et al. 2006; Greicius et al. 2003; Gusnard and Raichle 2001; Zhong et al. 2014).

Among the indices used in these studies, blood oxygenation level-dependent (BOLD) signal changes in ALFF have only been investigated for a single voxel. For ReHo, only synchronized changes in the BOLD signals of local brain regions have been studied (Yuan et al. 2016). In the FC, different seed points and their undirected relationships to other brain regions have also been studied. Although such research has provided insights into multiple brain regions, the human brain produced cognition depends on knowledge of its large-scale organization (Bressler and Menon 2010); thus, changes in a single voxel or a local brain region cannot fully explain changes in overall brain function. Certain fMRI studies have proposed completely contradictory conclusions (Fox et al. 2005; Greicius et al. 2003; Greicius and Menon 2004; Honey et al. 2007).

In 2011, Menon proposed the "triple networks" concept (Menon 2011), which includes the default-mode network (DMN), salience network (SN), and executive control network (ECN). The DMN and its core regions, which primarily include the MPFC, PCC, inferior parietal cortex (IPC), inferior temporal cortex (ITC) and the hippocampal formation (Buckner et al. 2008; Zhong et al. 2014), play an important role in monitoring the internal mental landscape (Gilbert et al. 2007; Mitchell et al. 2006). The SN is primarily anchored in the dorsal ACC (dACC) and plays an important role in the attentional capture of biologically and cognitively relevant events and subsequent engagement of frontoparietal systems for working memory and higher-order cognitive control (Menon and Uddin 2010; Sridharan et al. 2008). The ECN is a frontoparietal system anchored in the dorsolateral prefrontal cortex (dlPFC) and lateral posterior parietal cortex (PPC) (Habas et al. 2009; Seeley et al. 2007). The ECN is crucial for actively maintaining and manipulating information in working memory, rule-based problem solving and decision-making in the context of goal-directed behavior (Koechlin and Summerfield 2007; Muller and Knight 2006). The triple networks systematically engaged in mediation of cognition (Smith et al. 2009). This model provides a common framework for examining the stable and reliable patterns of large-scale connectivity (Menon 2011). The ECN and SN typically show an increase in activation during stimulus-driven cognitive and affective information processing, whereas the DMN shows decreased activation during tasks of self-referential and stimulus-independent memory recall.

Many studies have confirmed that the connectivity of these three networks are abnormal in different neurological diseases and mental disorders, including AD (Menon 2011). However, studies have not previously examined whether indices based on the three networks can be used to identify neuroimaging biomarkers for aMCI detection.

Granger causality analysis (GCA) is a method for investigating whether the past value of a time series in one brain region can correctly predict the current value of another region

based on multiple linear regressions. Recently, Zang et al. (2012) proposed the use of a signed-path coefficient from linear regression to measure directed interactions between brain regions. Positive and negative path coefficients indicate that the previous activity of a brain region can predict increased and decreased present activity in another region, respectively. Miao et al. (2011) used GCA to identify abnormal patterns in DMN hubs in AD.

In the present study, healthy control (HC), aMCI and AD subjects were analysed, and changes in directed FC (or effective connectivity) among the three networks in the three groups were studied. The directed FC indices were determined using GCA. The ultimate goal of the present analysis was to identify which method, brain region, and connection yield the most sensitive biomarkers for aMCI.

Materials and methods

Demographic and clinical assessments

AD and aMCI patients were recruited from the Memory Clinic of Zhejiang Provincial People's Hospital between January 2014 and December 2015. The HC subjects were volunteers who were primarily enrolled from the health promotion center of the hospital. All participants were right-handed and asked to provide written informed consent. All applied procedures were approved by the local Ethics Committee of Zhejiang Provincial People's Hospital (*Permit Number: 2012KY002*).

The patients received a standard dementia screening that included medical history, physical, and neurological examinations, screening of laboratory tests, neuropsychological testing, and brain MRI. Patients with AD met the revised NINCDS-ADRDA (National Institute of Neurological and Communicative Disorders and Stroke and the Alzheimer's Disease and Related Disorders Association) criteria for "probable AD" (McKhann et al. 2011). Neuropsychological tests were assessed using the Mini Mental State Examination (MMSE) (Folstein et al. 1975) and Montreal Cognitive Scale (MoCA). Patients with AD had a MMSE score ≤ 24 and a MoCA score ≤ 26.

Subjects with aMCI exhibited memory impairment but did not meet the criteria for dementia. The following criteria were used for the identification and classification of subjects with aMCI (Rivas-Vazquez et al. 2004): 1) complain of impaired memory; 2) MMSE score > 24 and ≤27; 3) maintain normal performance.

The criteria for HC subjects were: 1) no neurological or psychiatric disorders, such as stroke, depression, or epilepsy; 2) no neurological deficiencies, such as visual or hearing loss; 3) no abnormal infarction or focal lesion on conventional brain MR imaging.

For all subjects, exclusion criteria were: 1) vascular dementia or mixed dementia; 2) diseases that may cause memory loss such as Parkinson's disease, severe anemia, and cancer; 3) previous treatment with psychoactive substances; 4) any other types of dementia such as Pick disease, dementia with Lewy bodies, paresis of the insane or positive syphilis antibody with absence of paresis of the insane; 5) mental and nervous system diseases, hypertension, diabetes, and other severe physical diseases; 6) alcohol dependence, substance abuse, or a history of head trauma; 7) drug allergy, intolerance to scanning, or metal artifacts; or 8) high signal lesions with a diameter > 5 mm or more than 4 lesions with diameter < 5 mm using T2-FLAIR.

fMRI acquisition protocols

MRI data acquisition was performed using a Siemens Trio3-Tesla scanner equipped with a 12-channel phased-array head coil (Siemens, Erlangen, Germany) at Zhejiang Provincial People's Hospital. The participants were instructed to be still during the sessions, to keep their eyes closed but not fall asleep, and to relax. Resting-state functional images were collected axially using an echo-planar imaging (EPI) sequence with the following settings: 31 axial slices; thickness/gap, 3.2/0.8 mm; in-plane resolution, 64 × 64; repetition time (TR); 2000 ms; echo time (TE), 30 ms; flip angle, 90°; field of view (FOV), 220 mm × 220 mm; voxel size, 3 mm × 3 mm × 4 mm; 240 volumes (8 min). Three-dimensional T1- magnetization-prepared rapid gradient echo (MPRAGE) sagittal images were collected using the following parameters: 192 sagittal slices; slice thickness/gap, 1/0 mm; in-plane resolution, 256 × 256; TR, 1380 ms; TE, 2.6 ms; inversion time, 800 ms; flip angle, 15°; FOV, 256 mm × 256 mm; and voxel size, 1 mm × 1 mm × 1 mm.

Data pre-processing

The fMRI data were pre-processed using DPARSFA v2.3 (http://rfmri.org/DPARSF) and REST v1.8 (http://www.restfmri.net) based on SPM8 (http://www.fil.ion.ucl.ac.uk/spm) with MATLAB 2012a (MathWorks, Inc., Natick, MA, USA). Data pre-processing included the following steps: removal of the first four time points, allowing the longitudinal magnetization to reach a stable state and the participants to get used to the scanning environment; slice timing correction; head motion correction; spatial normalization to the Montreal Neurological Institute (MNI) space; rs-fMRI images resampling with voxels of 3 mm × 3 mm × 3 mm; spatial smoothing performed using an isotropic Gaussian kernel (FWHM = 6 mm); temporal filtering (0.01–0.08 Hz); removal of linear and quadratic trends; regression of covariates, including the global signal, a time series of the white matter and cerebrospinal fluid, and six affine motion parameters. The exclusion criterion

for excessive head motion was >2.0-mm translation or >2.0° rotation in any direction. Details of data pre-processing were reported in our previous study (Yu et al. 2016).

GCA

We followed Zang et al.'s (2012) extended vector AR model as follows:

$$Y^t = \sum_{k=1}^{p} A^k X^{(t-k)} + \sum_{k=1}^{p} B^k Y^{(t-k)} + CZ^t + E^t \quad (1)$$

$$X^t = \sum_{k=1}^{p} A'^k Y^{(t-k)} + \sum_{k=1}^{p} B'^k X^{(t-k)} + C' Z^t + E'^t \quad (2)$$

where X^t and Y^t represent two time series, A^k (formula (1)) and A'^k(formula (2)) are signed path coefficients, B^k(formula (1)) and B'^k(formula (2)) use auto regression, E^t(formula (1)) and E'^t (formula (2)) are residuals, and Z^t represents the covariates (e.g., head motion, global trend, and time series from certain brain areas). The time series X^t significantly Granger-causes time series Y^t if the signed path coefficient A^k is significantly larger or smaller than zero. Conversely, Y^t can be defined as significantly Granger-causing X^t if the signed path coefficient A'^k is significantly larger or smaller than zero.

Connectivity Degree of the Network:

In order to further explore the functional connectivity between the three networks, we defined a calculation for the network analysis as follows:

$$\Gamma_{MN} = \sum_{i=1}^{n} \sum_{j=1}^{m} \eta ij$$

where Γ_{mn} is the connectivity degree between the two networks M and N; m and n denote the number of nodes in the networks M and N, respectively; ηij denotes the interregional connectivity between nodes i and j, defined as $\eta ij = e^{-\xi dij}$; i represents the node of the network M; j is the node in the network N. The larger the value of Γ_{MN}, the greater the increase in functional connectivity between the two networks, representing excitatory connectivity. The negative value of Γ_{MN} represents decreased functional connectivity, meaning inhibitory connectivity (Zheng et al. 2015).

A region of interest (ROI) for the DMN was placed at the PCC (centring at $\chi = 0, y = -53, z = 26$), as in a previous GCA study (Hedden et al. 2009). The ROI for the SN was placed at the dACC (centring at $\chi = -6, y = 18, z = 30$), as in a previous GCA study (Seeley et al. 2007). The ROI of the ECN was placed at the dlPFC (centring at $\chi = 30, y = 12, z = 60$), as in a previous GCA study (Seeley et al. 2007). All ROI coordinates were in MNI space.

Voxel-wise GCA was performed using REST-GCA in the REST toolbox (http://www.restfmri.net). After obtaining the GCA map for each subject, standardization was performed by removing the whole-brain mean and dividing by the whole-brain standard deviation. The position of the three seed points is illustrated in Supplemental Fig. 1. In addition, estimation of the directed connectivity was based on the models shown in Supplemental Fig. 2.

Statistical analyses

A one-way analysis of covariance (ANCOVA) was used to compare age, education level and MMSE score among the AD/aMCI/HC groups. MoCA score comparison between the AD and aMCI groups was assessed by two-sample

Table 1 Demographics and neuropsychological performances of the AD, aMCI and healthy control patients

	AD	MCI	HC	Group comparison *P*-value (X^2 or *F* -value)
N	30	14	18	N/A
Age (years, mean ± SD)	72.83 ± 9.25	68.79 ± 8.99	73.78 ± 9.92	0.29(1.247[a])
Gender (M: F)	15:15	9:5	6:12	0.21(3.08[b])
Handedness (R: L)	30:0	14:0	18:0	N/A
Education (years, mean ± SD)	6.87 ± 3.68	9.57 ± 4.91	7.39 ± 4.91	0.16(1.88[a])
MMSE score (mean ± SD)	15.93 ± 5.34	26.00 ± 0.88	29.56 ± 0.51	< 0.001(82.64)*
MOCA score (mean ± SD)	10.63 ± 4.89	22.29 ± 1.86	–	< 0.001(63.02[a])*

A one-way analysis of covariance (ANCOVA) was used to compare age, education level and MMSE score among the AD/aMCI/HC groups. The MoCA score was calculated using two-sample independent *t*-tests; Fisher's exact test was used to assess the sex ratio between the three groups. *P*-values were adjusted for multiple comparisons.

AD Alzheimer's disease, *aMCI* amnestic mild cognitive impairment, *HC* healthy controls, *SD* standard deviation, *MMSE* mini mental state evaluation, *MoCA* Montreal cognitive scale

*$P<0.05$ for the differences between groups

[a] X^2 value

[b] *F* value

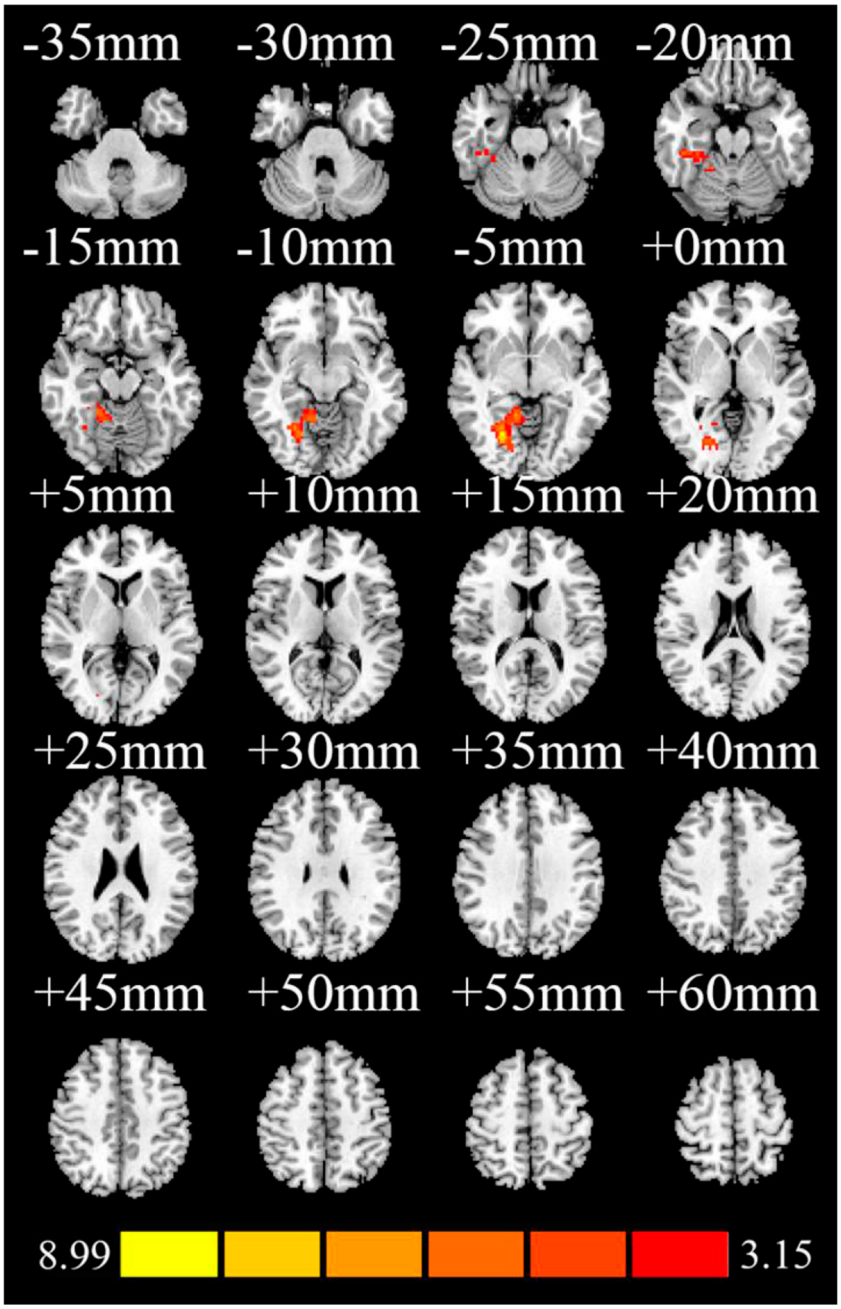

Fig. 1 Significant differences in GCA results (directed connectivity from the PCC to the whole brain, *x2y*, red). The *F*-test was used, with threshold set to $P < 0.05$ with the AlphaSim correction (individual $P < 0.05$, cluster size >228 mm^3) with the color scale representing the ranges off-values. The aberrant regions included the lingual gyrus, fusiform gyrus, cerebellum_4_5 and parahippocampal gyrus

independent *t*-tests. Gender ratio was examined by Fisher's exact test. $P < 0.05$ was considered statistically significant.

We performed voxel-wise group comparisons to assess potential group differences in seed-based GCA, and one-way analysis of variance (ANOVA) was used for this analysis. Unless specified, Monte Carlo simulations using the AlphaSim were used to derive an appropriate combination of voxel-based significance and cluster extent required to reach a corrected significance threshold of $P < 0.05$, which considered the effective smoothness as estimated directly from our pre-processed data (http://afni.nimh.nih.gov/pub-/dist/doc/manual/AlphaSim.pdf). To further investigate the differences between groups, regions that showed significant differences in the above-mentioned ANOVA were set as ROIs. The ROIs were spheres that presented the peak voxel as the centre with a radius of 6 mm. Average GC values were extracted from the ROIs; for each ROI, two-sample *t*-tests were performed for between-group comparisons with Bonferroni correction, and a significance level of 0.05/3 was set for *P* values. If significant results were not observed, the threshold values were further decreased to $P < 0.01$, and not corrected for multiple comparisons (the cluster size threshold was set to be larger than 40).

Table 2 Significant differences in the GCA results (PCC to the whole brain, x2y) between the AD/HC/aMCI groups

Regions	Hemisphere	BA	Number of voxels	Peak activation strength (F)	Peak coordinates		
					x	y	z
Lingual gyrus, fusiform gyrus, Cerebelum_4_5, parahippocampal gyrus	R	/	284	10.1591	24	−69	−3

The *F*-test was used, with threshold set to $P < 0.05$ with the AlphaSim correction (cluster size >228 mm^3). Averaged GC value was extracted from the ROI, for which a two-sample *t*-test was performed for between-group comparisons, with the *P*-value set at a significance level of 0.05/3. The degrees of freedom in AD/aMCI, AD/HC, and aMCI/HC group comparisons were 43, 47 and 31, respectively. The aberrant regions included the lingual gyrus, fusiform gyrus, cerebellum_4_5, and parahippocampal gyrus. The ROI was extracted from the right lingual gyrus (centring at $\chi = 24, y = -69, z = -3$)

Results

Demographic and clinical data

Two patients with AD had incomplete data. Data of 12 AD, 2 aMCI and 2 HC subjects could not be used due to the presence of artefacts. The remaining 4 AD participants, 1 aMCI participant and 1 HC participant were eliminated from the analysis due to excessive head movement. Consequently, the data of 30 AD (mean age, 72.83 ± 9.25 years; 15 males, MMSE, 15.93 ± 5.34), 14 aMCI (mean age, 68.79 ± 8.99 years; 9 males, MMSE, 26.00 ± 0.88), and 18 HC (mean age, 73.78 ± 9.92 years; 6 males, MMSE, 29.56 ± 0.51) participants were used for the subsequent analysis. The clinical and demographic data are listed in Table 1. Significant differences were not observed among the three groups with respect to gender, age, and education level ($P > 0.05$), and MMSE and MoCA scores were significantly different among the groups ($P < 0.05$).

GCA

From PCC to other regions (*x2y*, means directed connectivity from the seed point to whole brain regions; where x represents seed point, and y represents other brain regions).

Figure 1 and Table 2 show significant differences in GC among the three groups with respect to directed connectivity from the PCC seed points to other brain regions (*y2x*, means directed connection from whole brain regions to the seed point; where y represents other brain regions, and x represents the seed point). The different regions were concentrated in the right parahippocampal gyrus within the DMN as well as the lingual and fusiform gyri. The ROI was extracted from the right lingual gyrus (peak *Z*-GC centring at $\chi = 24, y = -69, z = -3$)(Fig. 1 and Table 2). A three-group comparison showed that the GC values of the AD group were higher than those observed for the other two groups, which exhibited excitatory connectivity (GC value increased) (Table 3). However, the aMCI group exhibited inhibitory connectivity (the GC value decreased significantly from that of the AD group) (Fig. 2a).

Table 3 The GC results comparison of three-group in AD/HC/aMCI

Regions	Connections	Value(Mean ± SD)			*t*-value			*P*-value		
		A	B	C	A-B	A-C	B-C	A-B	A-C	B-C
Lingual gyrus(R)	GC(PCC-x2y)	0.40 ± 0.18	−0.36 ± 0.23	−0.94 ± 0.30	2.52	3.89	1.50	0.0153*	0.0004*	0.1438
Thalamus(R)	GC(PCC-y2x)	0.49 ± 0.17	0.14 ± 0.25	−0.88 ± 0.26	1.14	4.37	2.79	0.2612	<0.0001*	0.009*
Insula	GC(dACC-x2yROI 1)	−0.25 ± 0.21	−1.14 ± 0.23	0.14 ± 0.24	2.71	1.13	3.76	0.0094*	0.2761	0.0007*
Parietal(L)	GC(dACC-x2yROI 2)	−0.31 ± 0.19	0.03 ± 0.35	1.12 ± 0.34	0.92	3.92	2.16	0.3641	0.0003*	0.039
Parahippocampal gyrus (L)	GC(dlPFC-x2y ROI 1)	-0.69 ± 0.35	−0.85 ± 0.28	1.18 ± 0.36	0.33	3.27	4.49	0.7465	0.0022*	<0.0001*
Superior medial frontal gyrus(L)	GC(dlPFC-x2y ROI 2)	0.13 ± 0.35	0.55 ± 0.47	−2.41 ± 0.46	0.71	4.14	4.38	0.4844	0.0002*	<0.0001*

Two-sample *t*-tests were performed for between-group comparisons with Bonferroni corrections, and *P-value*s were set at a significance level of 0.0166 (0.05/3). Data are mean ± standard deviation (SD)

Key: *A,* Alzheimer's disease group (AD group); *B*, Healthy control group (HC group); *C,* Amnestic mild cognitive impairment group (aMCI group); *GC* Granger causality; *PCC* posterior cingulate cortex; *dACC* dorsal anterior cingulate cortex; *dlPFC* dorsolateral prefrontal cortex; *R* right; and *L* left

*denotes significant differences between groups

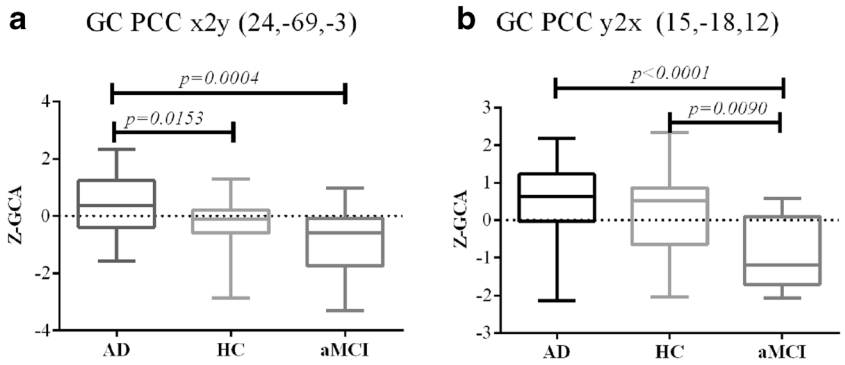

Fig. 2 GC analysis results. **a**, Pair-wise comparisons for significantly different GC values extracted from the ROI, which was the right lingual gyrus (centring at $\chi = 24, y = -69, z = -3$) from the PCC to other regions (*x2y*) among the AD/aMCI/HC groups; **b**, pair-wise comparisons for the significantly different GC values extracted from the ROI, which was the right thalamus (centring at $\chi = 15, y = -18, z = 12$) from other regions to the PCC (*y2x*) among the AD/aMCI/HC groups

From other regions to PCC(y2x)

The GC from other brain regions to PCC seed points differed among the three groups. This difference primarily appeared in the right thalamus within the DMN, with peak *Z*-GC centring at $\chi = 15, y = -18, z = 12$ (Fig. 3 and Table 4). A significant difference was observed between the aMCI group and the other two groups; however, significant differences were not observed between the AD and HC groups (Table 3). Group comparison showed that the AD and HC groups exhibited excitatory connectivity, whereas the aMCI group exhibited inhibitory connectivity (Fig. 2b).

From SN to other regions(x2y)

Aberrant directed connectivity was observed from the SN, with the dACC as a representative seed point to the whole-brain network. This aberrant activity was observed in the corpus striatum within the SN, including the caudate nucleus and putamen (Fig. 4). The ROI 1 was extracted from the left insula (the peak *Z*-GC centring at $\chi = -33, y = 3, z = 6$) (Table 5). The directed connectivity within the SN exhibited excitatory characteristics for the aMCI group, which showed a significant difference from inhibitory connectivity in the HC group. The GC of the AD group also showed inhibitory connectivity significantly higher than that of the HC group (Fig. 5a, Table 3). In addition, ROI 2 exhibiting significant differences was extracted from the ECN at the left parietal cortex peak *Z*-GC, centring at $\chi = -27, y = -60, z = 48$ (Table 5). This result indicates a significant difference in the directed connectivity from the SN to the ECN. This SN-ECN connectivity manifested as markedly increased excitatory connectivity in the aMCI group and exhibited a significant difference from that of the other two groups (Fig. 5b, Table 3).

No significant difference in connectivity was observed among the groups from other brain regions to the dACC (*y2x*).

From ECN to other regions (x2y)

Differences were detected in the directed connectivity of the ECN with the dlPFC as the representative seed point to the whole-brain network. The aberrant directed connectivity from the ECN to the DMN included the left parahippocampal gyrus, hippocampus, lentiform nucleus, temporal middle gyrus, lingual gyrus and pallidum, with the peak *Z*-GC extracted from the left parahippocampal gyrus centring at $\chi = -15, y = -33, z = -6$. The aberrant directed connectivity from the ECN to SN included the bilateral superior medial frontal gyrus, superior frontal gyrus and supplementary motor area, with the peak *Z*-GC extracted from the superior medial frontal gyrus centring at $\chi = 6, y = 42, z = 45$ (Fig. 6, Table 6). The ECN-DMN connectivity was excitatory in the aMCI group but was inhibitory in the AD and HC groups. A significant difference was observed between aMCI and the other two groups (Fig. 5c, Table 3). Changes in the connectivity of the ECN-SN were observed in all three groups. The AD and HC groups showed significant excitatory connectivity, whereas the aMCI group exhibited significant inhibitory connectivity (Fig. 5d, Table 3).

No significant connectivity differences from other brain regions to the dlPFC were found between the groups (*y2x*).

Discussion

Menon et al. proposed that dysregulated interactions within and among three core brain networks (i.e., ECN, DMN, and SN), which closely correlate with aberrant saliency mapping and cognitive dysfunction in psychopathology, including dementia (Menon 2011). Our results are consistent with this conclusion and show that directed connectivity can reveal a series of compensational or pathological changes in aMCI, with GC as an indicator. GCA showed significant differences among the aMCI, AD and HC groups in this study. We believe

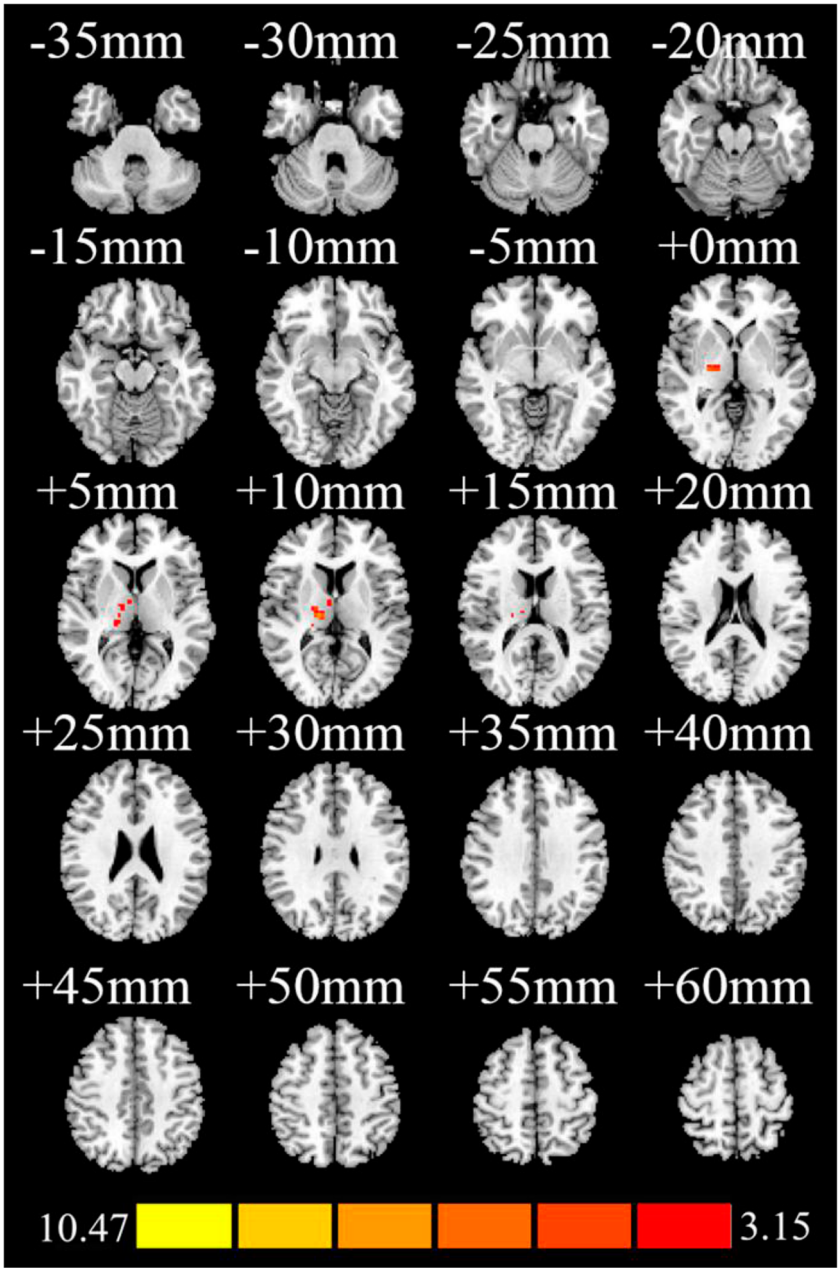

Fig. 3 Significant differences in the GCA results (directed connectivity from other regions to PCC, *y2x,* red). The *F*-test was used, with threshold set to $P < 0.05$ with the AlphaSim correction (individual $P < 0.05$, cluster size >228 mm^3) with the color scale representing the ranges off-values. The aberrant region was the right thalamus

that directed connectivity within networks is sensitive and may serve as a neuroimaging biomarker for aMCI.

The DMN performs inhibitory activation during cognitive processes. When there are pathological changes in brain

Table 4 Significant differences in GCA results (whole brain to PCC, y2x) between the AD/HC/aMCI groups

Regions	Hemisphere	BA	Number of voxels	Peak activation strength (F)	Peak coordinates		
					x	y	z
Thalamus	R	/	52	9.6077	15	−18	12

The *F*-test was used, with threshold set to $P < 0.05$ with the AlphaSim correction (cluster size >228 mm^3). The averaged GC value was extracted from the ROI, for which a two-sample *t*-test was performed for between-group comparisons, with a *P*-value set at a significance level of 0.05/3. The degrees of freedom in AD/aMCI, AD/HC, and aMCI/HC group comparisons were 43, 47 and 31, respectively. The ROI was extracted from the right thalamus (centring at $\chi = 15, y = -18, z = 12$)

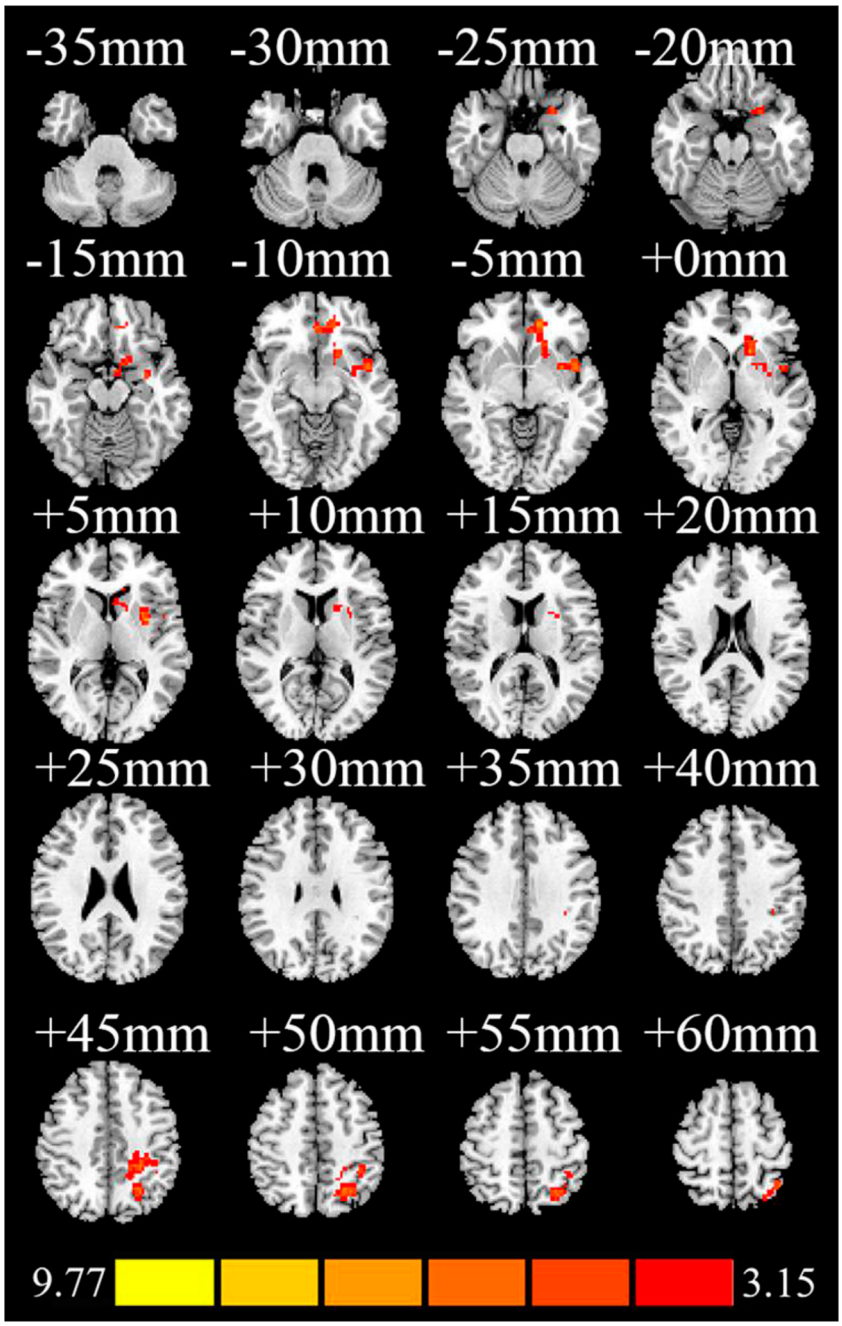

Fig. 4 Significant differences in GCA results (directed connectivity from the dACC to the whole brain, *x2y*, red). The *F*-test was used, with threshold set to $P < 0.05$ with the AlphaSim correction (individual $P < 0.05$, cluster size >228 mm^3) with the color scale representing the ranges off-values. The aberrant regions included the left insula, putamen, caudate, frontal middle orb gyrus, parietal superior/inferior gyrus and postcentral gyrus

networks, increased activation is observed. In the current study, the directed connectivity within the DMN as well as that from the DMN to the visual cortex (i.e., the lingual and fusiform gyri) differed among the three groups. The AD group exhibited excitatory connectivity, while the aMCI and HC groups exhibited markedly decreased connectivity (Fig. 2c). The GC of aMCI was the lowest, and characterized by compensatory connectivity. In addition, the directed connectivity from the thalamus to the DMN also exhibited an abnormal inhibitory effect in aMCI that was interpreted as a type of adaptive protective mechanism (Fig. 2d). The altered FC from the DMN to the lingual and fusiform gyri could be the principal cause of deficient memory, and may reflect a breakdown of visual-related cortical networks in AD.

As mentioned above, the SN typically shows excitation during stimulus-driven cognitive processing, whereas the abnormal connectivity observed in aMCI is inhibitory. Previous research has shown that the excitatory directed connectivity within the SN represented by the dACC seed point appears in aMCI (Fig. 6a). The excitatory connectivity of the SN-ECN connection was only found in the aMCI group under the same conditions (Fig. 6b). However, the AD group exhibited declined inhibitory connectivity, which may be explained as follows: the SN is responsible for advanced cognitive

Table 5 Significant differences in GCA results (dACC to the whole brain, x2y) between the AD/HC/aMCI groups

Regions	Hemisphere	BA	Number of voxels	Peak activation strength (F)	Peak coordinates		
					x	y	z
Insula, putamen, caudate, frontal middle orb gyrus	L	/	346	7.9824	−33	3	6
Parietal superior/inferior gyrus, postcentral gyrus	L	7	232	8.2957	−27	−60	48

The *F*-test was used, with threshold set to $P < 0.05$ with the AlphaSim correction (cluster size >228 mm^3). Average GC values were extracted from the ROIs, for which two-samples *t*-tests were performed for between-group comparisons, with *P*-value set at a significance level of 0.05/3. The degrees of freedom in AD/aMCI, AD/HC, and aMCI/HC group comparisons were 43, 47 and 31, respectively. The first line represents the within-SN connectivity from the dACC to other regions, such as the insula, putamen, caudate and frontal middle orb gyrus. The second line represents aberrant connectivity from the SN to the ECN such as the left parietal superior/inferior gyrus and postcentral gyrus. The ROI 1 (first line) was extracted from the left insula (centring at $\chi = -33, y = 3, z = 6$). The ROI 2 (second line) was extracted from the left parietal (centring at $\chi = -27, y = -60, z = 48$)

functions, such as social and affective information (Botvinick et al. 2004), which are increased upon activation. For example, SN hyperactivity has been correlated with anxiety disorder (Stein et al. 2007). In the aMCI stage (in which the MMSE values do not meet the diagnosis standard of AD), anxiety and depression are the prominent accompanying symptoms (Orgeta et al. 2015) and may increase the excitatory-directed connectivity of the SN. Another possible reason could be compensatory mechanisms. The AD group exhibited decreased inhibitory connectivity, which may indicate an inability to compensate. The directed connectivity from the dACC seed point to other brain regions was concentrated in the insula, putamen, caudate nucleus, parietal lobe, and superior/inferior gyrus (Table 6). These brain regions are primarily

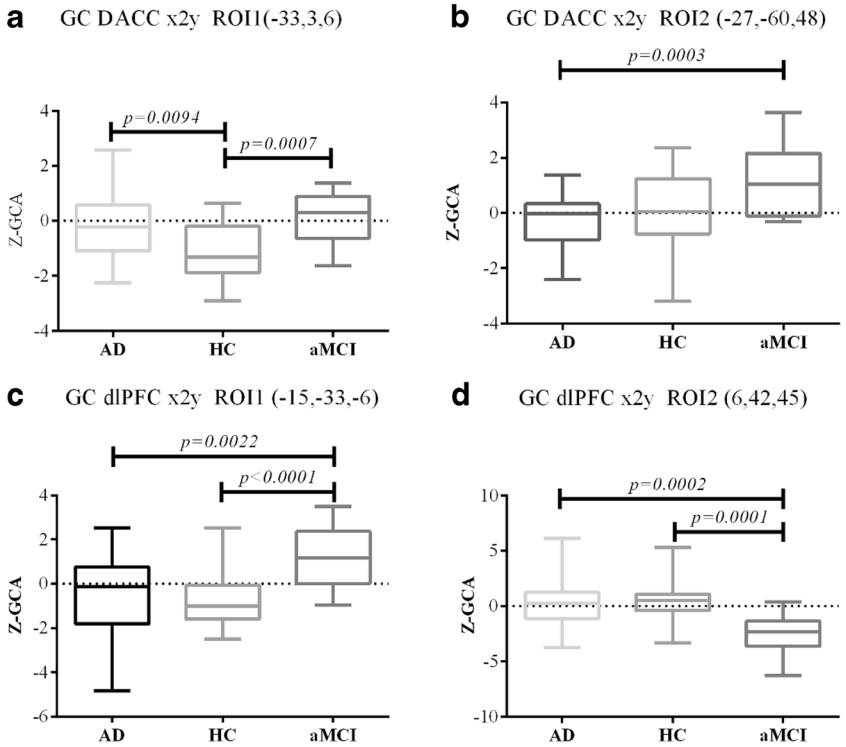

Fig. 5 GCA results of SN/ECN: **a**, Pair-wise comparisons for significantly different GC values extracted from ROI 1, which was the left insula (centring at $\chi = -33, y = 3, z = 6$) from the dACC to other regions within the SN among the AD/aMCI/HC groups; **b**, pair-wise comparisons for significantly different GC values extracted from ROI 2, which was the left parietal (centring at $\chi = -27, y = -60, z = 48$) from the SN to the ECN among the AD/aMCI/HC groups; **c**, pair-wise comparisons for the significantly different GC values extracted from ROI 1, which was the left parahippocampal gyrus (centring at $\chi = -15, y = -33, z = -6$) from the ECN to the DMN among the AD/aMCI/HC groups; and **d**, pair-wise comparisons for the significantly different GC values extracted from ROI 2, which was the left superior medial frontal gyrus (centring at $\chi = 6, y = 42, z = 45$) from the ECN to the SN among the AD/aMCI/HC groups

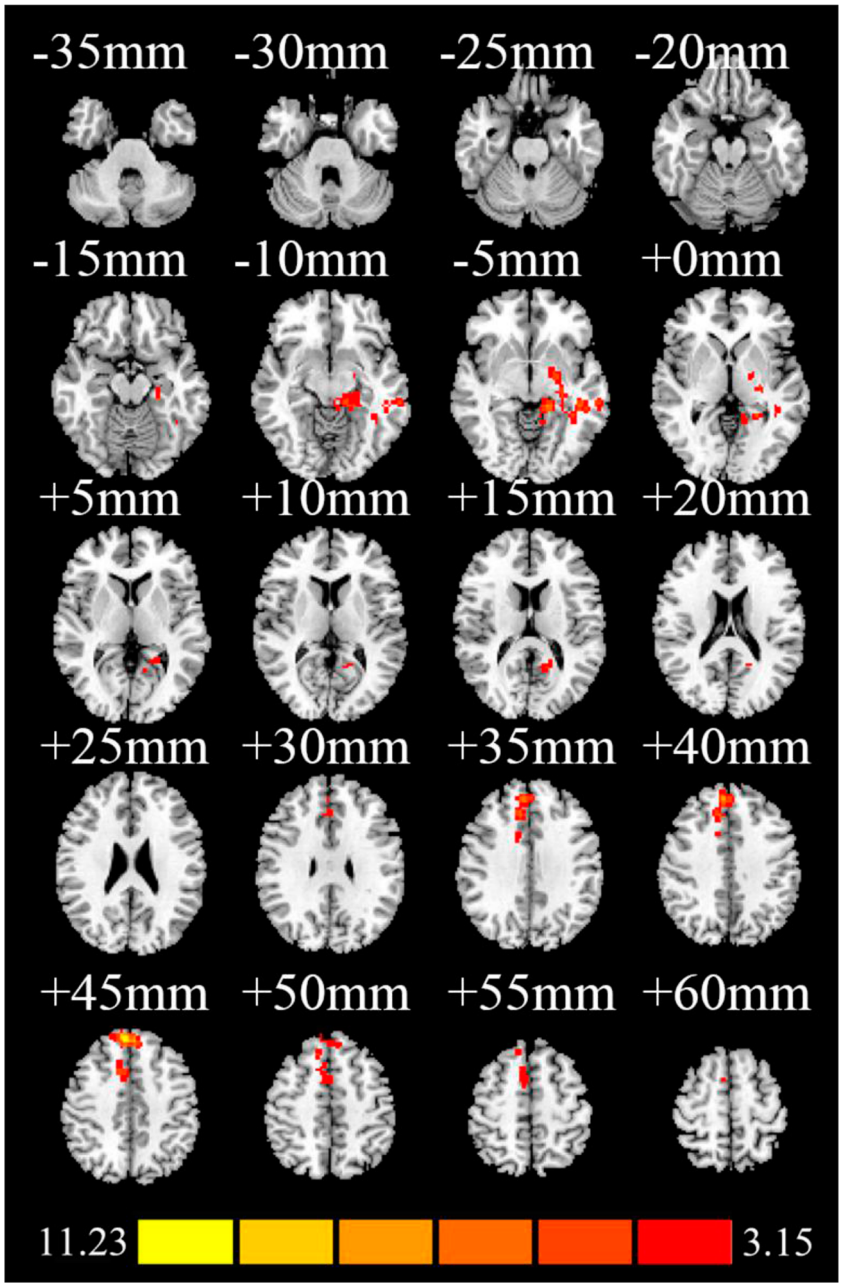

Fig. 6 Significant differences in GCA results (directed connectivity from the dlPFC to the whole brain, *x2y*, red). The *F*-test was used, with threshold set to $P < 0.01$ (uncorrected, cluster size >40 mm^3) with the color scale representing the ranges off-values. The aberrant regions included the left parahippocampal gyrus, hippocampus, lentiform nucleus, temporal middle gyrus, lingual gyrus, pallidum, bilateral superior medial frontal gyrus, superior frontal gyrus, and supplementary motor area

correlated with cognitive control, attention, emotion, and short-term memory (Beaty et al. 2015; Gasquoine 2014; Todd and Marois 2004), which are associated with the symptoms of AD.

The ECN shows excitatory connectivity during the affective information procession, which is similar to the observed activity in the SN. For the directed connectivity of the ECN, including the dlPFC (as the representative seed point) and the DMN, several differences were detected in multiple brain regions, including the hippocampus/parahippocampal gyrus, lentiform nucleus, and temporal middle gyrus. The excitatory connectivity in the aMCI group may represent another type of compensatory protection. The ECN showed increased activation during cognitive and affective information processing. However, the directed connectivity from the ECN to parts of the SN, such as the supplementary motor area, showed inhibitory connectivity in the aMCI group. This may be the result of feedback inhibition, which deserves further attention. Other data have demonstrated that memory-encoding regions involve the hippocampus, precuneus, PCC and lingual gyrus, prefrontal lobe, parietal lobe and occipital lobe (Schwindt and Black 2009; Wang et al. 2007). Thus, our finding of aberrant connectivity in these brain regions in AD and aMCI subjects was consistent with previous studies.

The SN can initiate brain networks, guide the ECN and DMN to execute cognitive tasks, and help target brain regions

Table 6 Significant differences in GCA results (dlPFC to the whole brain, x2y) between the AD/HC/aMCI groups

Regions	Hemisphere	BA	Number of voxels	Peak activation strength (F)	Peak coordinates		
					x	y	z
Parahippocampal gyrus, hippocampus, lentiform nucleus, temporal middle gyrus, lingual gyrus, pallidum	L	/	288	8.9627	−15	−33	−6
Superior medial frontal gyrus, superior frontal gyrus, supplementary motor area	L/R	6/8/9	327	12.8440	6	42	45

The *F*-test was used, with threshold set to $P < 0.01$ (uncorrected, cluster size >40 mm^3). Average GC values were extracted from the ROIs, for which two-sample *t*-tests were performed for between-group comparisons, with *P*-values set at a significance level of 0.01/3. The degrees of freedom in AD/aMCI, AD/HC, and aMCI/HC group comparisons were 43, 47 and 31, separately. The first line represents the aberrant directed connectivity from the ECN to the DMN such as the left parahippocampal gyrus, hippocampus, lentiform nucleus, temporal middle gyrus, lingual gyrus and pallidum. The second line represents the aberrant directed connectivity from the ECN to SN, such as the bilateral superior medial frontal gyrus, superior frontal gyrus, and supplementary motor area. The ROI 1 (first line) was extracted from the left parahippocampal gyrus (centring at $\chi = -15, y = -33, z = -6$). The ROI 2 (second line) was extracted from the left superior medial frontal gyrus (centring at $\chi = 6, y = 42, z = 45$)

to respond appropriately to stimulation, thereby playing vital roles in cognitive task performance (Menon 2011). Studies have suggested that aberrant connectivity within the DMN and from the DMN to other brain regions can be considered a biological marker of AD (Miao et al. 2011; Zhong et al. 2014). The current findings confirm this hypothesis and further demonstrate that aberrant connectivity in other core regions (ECN and SN) can be detected in AD and aMCI patients. The group of aMCI patients exhibited particularly significant differences between the AD and HC groups, and fMRI studies based on the "triple networks" concept have provided new insights into the large-scale neural networks of intrinsic connectivity in AD and aMCI. We believe that such studies may provide sensitive neuroimaging biomarkers for aMCI. As a large-scale network, the three core networks interact with and feedback to each other. Except for the directed connectivity in DMN, we did not observe opposite-direction aberrant connectivity in the ECN and SN, although this may have been related to increased importance of the DMN network in AD. The medial temporal lobe within the DMN is one of the first brain regions to become altered in the progression AD.

The directed connectivity data obtained from GCA can differentiate between excitatory and inhibitory connectivity and distinguish the direction. This indicator can reveal aberrant connectivity at an early stage of the disease process when obvious declines in cognitive function have not been observed in subjects with aMCI. The differences observed on imaging in both inhibitory and excitatory connectivity may be characteristic of aMCI. The inhibitory connections occurred (i) from the PCC to the hippocampal formation within the DMN; and (ii) from the thalamus to the DMN. The excitatory connections occurred (i) from the dACC to the corpus striatum within the SN, (ii) from the SN to the ECN, and (iii) from the ECN to the DMN. We consider these connections compensatory effects in aMCI, representing potential high-sensitivity neuroimaging biomarkers for aMCI. The inhibitory connectivity from ECN to SN may be the result of feedback inhibition.

Our study had several limitations. The statistical analysis was challenging due to the relatively small sample size and disproportionate number of subjects, particularly in the aMCI and HC groups. Therefore, these findings should be interpreted with caution, and further studies are required to verify the results. AD patients were characterized by less education (years) than the other two groups, whereas significant differences were not observed among the three groups based on the level of education. However, these results do not completely exclude the influence of less education on the results obtained. In this study, only the GCA changes between important nodes of the three networks were studied; thus, the other seeds among the "triple networks" should be investigated in the future.

Future studies should better explore the relationship between cognitive function and disease stage using the Wisconsin card sorting test, language fluency test and trail making test. In addition, a longitudinal study that can better track changes in AD overtime and how they relate to changes in AD severity based on the triple networks model should be performed. Prospective studies should be conducted to investigate whether aMCI patients who show GCA abnormalities ultimately progress to AD.

Conclusion

Using GCA analytical techniques, we revealed variations in the connectivity of the three core networks (SN, ECN, and DMN) in the AD, aMCI and HC groups. Changes in directed connectivity were observed in all three groups. The directed (excitatory and inhibitory) connectivity obtained from the GCA could differentiate among the AD, aMCI, and control groups. These results suggest that the directed connectivity of inter-hemisphere connectivity is sensitive to changes in connectivity that manifest in early cognitive decline. Specifically, inhibitory connectivity within the DMN from the PCC to the hippocampal formation, inhibitory connectivity from the thalamus to the PCC, and excitatory within-SN connectivity from

the dACC to the striatum, the SN to the ECN, and the ECN to the DMN were observed. These results demonstrate that such aberrant connectivity may be used to differentiate between aMCI and HC, and likely reflect compensatory changes in aMCI. The inhibitory connectivity from to ECN to SN was difficult to interpret but may result from feedback inhibition. These findings suggest that changes in the triple networks may be used as sensitive neuroimaging biomarkers for the early detection of aMCI. Early detection would allow physicians to provide early interventions that decrease morbidity and mortality in patients with AD.

Acknowledgements This study is funded by the Zhejiang Provincial Natural Science Foundation of China (no. Y2091289, LY16H180007, LY13H180016) and the Science Foundation from Health Commission of Zhejiang Province (no. 2013RCA001, 2016147373, ZKJ-ZJ-1503). The funders had no role in study design, data collection and analysis, decision to publish, or preparation of the manuscript.

Compliance with ethical standards

Conflict of interest Enyan Yu, Zhengluan Liao, Yunfei Tan, Yaju Qiu, Junpeng Zhu, Zhang Han, Jue Wang, Xinwei Wang, Hong Wang, Yan Chen, Qi Zhang, Yumei Li, Dewang Mao, and Zhongxiang Ding declare that they have no conflict of interest.

Informed consent All procedures followed were in accordance with the ethical standards of the responsible committee on human experimentation (institutional and national) and the Helsinki Declaration of 1975, and the applicable revisions at the time of investigation. Informed consent was obtained from all patients. The study was approved by the institutional Ethics Committee number: 2012KY002.

References

Andreasen, J. T., & Redrobe, J. P. (2009). Nicotine, but not mecamylamine, enhances antidepressant-like effects of citalopram and reboxetine in the mouse forced swim and tail suspension tests. *Behavioural Brain Research, 197*(1), 150–156. doi:10.1016/j.bbr.2008.08.016.

Bai, F., Zhang, Z., Yu, H., Shi, Y., Yuan, Y., Zhu, W., et al. (2008). Default-mode network activity distinguishes amnestic type mild cognitive impairment from healthy aging: a combined structural and resting-state functional MRI study. *Neuroscience Letters, 438*(1), 111–115. doi:10.1016/j.neulet.2008.04.021.

Beaty, R. E., Benedek, M., Barry Kaufman, S., & Silvia, P. J. (2015). Default and executive network coupling supports creative idea production. *Scientific Reports, 5*, 10964. doi:10.1038/srep10964.

Binnewijzend, M. A., Schoonheim, M. M., Sanz-Arigita, E., Wink, A. M., van der Flier, W. M., Tolboom, N., et al. (2012). Resting-state fMRI changes in Alzheimer's disease and mild cognitive impairment. *Neurobiology of Aging, 33*(9), 2018–2028. doi:10.1016/j.neurobiolaging.2011.07.003.

Botvinick, M. M., Cohen, J. D., & Carter, C. S. (2004). Conflict monitoring and anterior cingulate cortex: An update. *Trends in Cognitive Sciences, 8*(12), 539–546. doi:10.1016/j.tics.2004.10.003.

Bressler, S. L., & Menon, V. (2010). Large-scale brain networks in cognition: emerging methods and principles. *Trends in Cognitive Sciences, 14*(6), 277–290.

Buckner, R. L., Andrews-Hanna, J. R., & Schacter, D. L. (2008). The brain's default network: anatomy, function, and relevance to disease. *Annals of the New York Academy of Sciences, 1124*, 1–38. doi:10.1196/annals.1440.011.

De Luca, M., Beckmann, C. F., De Stefano, N., Matthews, P. M., & Smith, S. M. (2006). fMRI resting state networks define distinct modes of long-distance interactions in the human brain. *NeuroImage, 29*(4), 1359–1367. doi:10.1016/j.neuroimage.2005.08.035.

Folstein, M. F., Folstein, S. E., & McHugh, P. R. (1975). "Mini-mental state". A practical method for grading the cognitive state of patients for the clinician. *Journal of Psychiatric Research, 12*(3), 189–198.

Fox, M. D., Snyder, A. Z., Vincent, J. L., Corbetta, M., Van Essen, D. C., & Raichle, M. E. (2005). The human brain is intrinsically organized into dynamic, anticorrelated functional networks. *Proceedings of the National Academy of Sciences of the United States of America, 102*(27), 9673–9678. doi:10.1073/pnas.0504136102.

Ganguli, M., Snitz, B. E., Saxton, J. A., Chang, C. C., Lee, C. W., Vander Bilt, J., et al. (2011). Outcomes of mild cognitive impairment by definition: a population study. *Archives of Neurology, 68*(6), 761–767. doi:10.1001/archneurol.2011.101.

Gasquoine, P. G. (2014). Contributions of the insula to cognition and emotion. *Neuropsychology Review, 24*(2), 77–87. doi:10.1007/s11065-014-9246-9.

Gilbert, S. J., Dumontheil, I., Simons, J. S., Frith, C. D., & Burgess, P. W. (2007). Comment on "wandering minds: the default network and stimulus-independent thought". *Science, 317*(5834), 43. doi:10.1126/science.1140801.

Greicius, M. D., & Menon, V. (2004). Default-mode activity during a passive sensory task: Uncoupled from deactivation but impacting activation. *Journal of Cognitive Neuroscience, 16*(9), 1484–1492. doi:10.1162/0898929042568532.

Greicius, M. D., Krasnow, B., Reiss, A. L., & Menon, V. (2003). Functional connectivity in the resting brain: a network analysis of the default mode hypothesis. *Proceedings of the National Academy of Sciences of the United States of America, 100*(1), 253–258. doi:10.1073/pnas.0135058100.

Gusnard, D. A., & Raichle, M. E. (2001). Searching for a baseline: Functional imaging and the resting human brain. *Nature Reviews: Neuroscience, 2*(10), 685–694. doi:10.1038/35094500.

Habas, C., Kamdar, N., Nguyen, D., Prater, K., Beckmann, C. F., Menon, V., et al. (2009). Distinct cerebellar contributions to intrinsic connectivity networks. *Journal of Neuroscience, 29*(26), 8586–8594. doi:10.1523/JNEUROSCI.1868-09.2009.

Hedden, T., Van Dijk, K. R., Becker, J. A., Mehta, A., Sperling, R. A., Johnson, K. A., et al. (2009). Disruption of functional connectivity in clinically normal older adults harboring amyloid burden. *Journal of Neuroscience, 29*(40), 12686–12694. doi:10.1523/JNEUROSCI.3189-09.2009.

Honey, C. J., Kotter, R., Breakspear, M., & Sporns, O. (2007). Network structure of cerebral cortex shapes functional connectivity on multiple time scales. *Proceedings of the National Academy of Sciences of the United States of America, 104*(24), 10240–10245. doi:10.1073/pnas.0701519104.

Koechlin, E., & Summerfield, C. (2007). An information theoretical approach to prefrontal executive function. *Trends in Cognitive Sciences, 11*(6), 229–235. doi:10.1016/j.tics.2007.04.005.

Li, S. J., Li, Z., Wu, G., Zhang, M. J., Franczak, M., & Antuono, P. G. (2002). Alzheimer disease: evaluation of a functional MR imaging index as a marker. *Radiology, 225*(1), 253–259. doi:10.1148/radiol.2251011301.

McKhann, G. M., Knopman, D. S., Chertkow, H., Hyman, B. T., Jack Jr., C. R., Kawas, C. H., et al. (2011). The diagnosis of dementia due to Alzheimer's disease: recommendations from the National Institute on Aging-Alzheimer's Association workgroups on diagnostic guidelines for Alzheimer's disease. *Alzheimers & Dementia, 7*(3), 263–269. doi:10.1016/j.jalz.2011.03.005.

Menon, V. (2011). Large-scale brain networks and psychopathology: a unifying triple network model. *Trends in Cognitive Sciences, 15*(10), 483–506. doi:10.1016/j.tics.2011.08.003.

Menon, V., & Uddin, L. Q. (2010). Saliency, switching, attention and control: a network model of insula function. *Brain Structure & Function, 214*(5–6), 655–667. doi:10.1007/s00429-010-0262-0.

Miao, X., Wu, X., Li, R., Chen, K., & Yao, L. (2011). Altered connectivity pattern of hubs in default-mode network with Alzheimer's disease: an Granger causality modeling approach. *PloS One, 6*(10), e25546. doi:10.1371/journal.pone.0025546.

Mitchell, J. P., Macrae, C. N., & Banaji, M. R. (2006). Dissociable medial prefrontal contributions to judgments of similar and dissimilar others. *Neuron, 50*(4), 655–663. doi:10.1016/j.neuron.2006.03.040.

Morris, J. C., Storandt, M., Miller, J. P., McKeel, D. W., Price, J. L., Rubin, E. H., et al. (2001). Mild cognitive impairment represents early-stage Alzheimer disease. *Archives of Neurology, 58*(3), 397–405.

Muller, N. G., & Knight, R. T. (2006). The functional neuroanatomy of working memory: contributions of human brain lesion studies. *Neuroscience, 139*(1), 51–58. doi:10.1016/j.neuroscience.2005.09.018.

Orgeta, V., Qazi, A., Spector, A., & Orrell, M. (2015). Psychological treatments for depression and anxiety in dementia and mild cognitive impairment: systematic review and meta-analysis. *British Journal of Psychiatry, 207*(4), 293–298. doi:10.1192/bjp.bp.114.148130.

Petersen, R. C., Thomas, R. G., Grundman, M., Bennett, D., Doody, R., Ferris, S., et al. (2005). Vitamin E and donepezil for the treatment of mild cognitive impairment. *New England Journal of Medicine, 352*(23), 2379–2388. doi:10.1056/NEJMoa050151.

Rivas-Vazquez, R. A., Mendez, C., Rey, G. J., & Carrazana, E. J. (2004). Mild cognitive impairment: new neuropsychological and pharmacological target. *Archives of Clinical Neuropsychology, 19*(1), 11–27.

Schwindt, G. C., & Black, S. E. (2009). Functional imaging studies of episodic memory in Alzheimer's disease: a quantitative meta-analysis. *NeuroImage, 45*(1), 181–190. doi:10.1016/j.neuroimage.2008.11.024.

Seeley, W. W., Menon, V., Schatzberg, A. F., Keller, J., Glover, G. H., Kenna, H., et al. (2007). Dissociable intrinsic connectivity networks for salience processing and executive control. *Journal of Neuroscience, 27*(9), 2349–2356. doi:10.1523/JNEUROSCI.5587-06.2007.

Smith, S. M., Fox, P. T., Miller, K. L., Glahn, D. C., Fox, P. M., Mackay, C. E., et al. (2009). Correspondence of the brain's functional architecture during activation and rest. *Proceedings of the National Academy of Sciences of the United States of America, 106*(31), 13040–13045.

Sorg, C., Riedl, V., Muhlau, M., Calhoun, V. D., Eichele, T., Laer, L., et al. (2007). Selective changes of resting-state networks in individuals at risk for Alzheimer's disease. *Proceedings of the National Academy of Sciences of the United States of America, 104*(47), 18760–18765. doi:10.1073/pnas.0708803104.

Sridharan, D., Levitin, D. J., & Menon, V. (2008). A critical role for the right fronto-insular cortex in switching between central-executive and default-mode networks. *Proceedings of the National Academy of Sciences of the United States of America, 105*(34), 12569–12574. doi:10.1073/pnas.0800005105.

Stein, M. B., Simmons, A. N., Feinstein, J. S., & Paulus, M. P. (2007). Increased amygdala and insula activation during emotion processing in anxiety-prone subjects. *American Journal of Psychiatry, 164*(2), 318–327. doi:10.1176/ajp.2007.164.2.318.

Todd, J. J., & Marois, R. (2004). Capacity limit of visual short-term memory in human posterior parietal cortex. *Nature, 428*(6984), 751–754. doi:10.1038/nature02466.

Wang, K., Liang, M., Wang, L., Tian, L., Zhang, X., Li, K., et al. (2007). Altered functional connectivity in early Alzheimer's disease: a resting-state fMRI study. *Human Brain Mapping, 28*(10), 967–978. doi:10.1002/hbm.20324.

Yu, E., Liao, Z., Mao, D., Zhang, Q., Ji, G., Li, Y., et al. (2016). Directed functional connectivity of posterior cingulate cortex and whole brain in Alzheimer's disease and mild cognitive impairment. *Current Alzheimer Research*.

Yuan, X., Han, Y., Wei, Y., Xia, M., Sheng, C., Jia, J., He, Y., et al. (2016). Regional homogeneity changes in amnestic mild cognitive impairment patients. *Neuroscience Letters, 629*, 1–8. doi:10.1016/j.neulet.2016.06.047.

Zang, Z. X., Yan, C. G., Dong, Z. Y., Huang, J., & Zang, Y. F. (2012). Granger causality analysis implementation on MATLAB: a graphic user interface toolkit for fMRI data processing. *Journal of Neuroscience Methods, 203*(2), 418–426. doi:10.1016/j.jneumeth.2011.10.006.

Zheng, H., Xu, L., Xie, F., Guo, X., Zhang, J., Yao, L., et al. (2015). The altered triple networks interaction in depression under resting state based on graph theory. *BioMed Research International, 2015*, 386326.

Zhong, Y., Huang, L., Cai, S., Zhang, Y., von Deneen, K. M., Ren, A., et al. (2014). Altered effective connectivity patterns of the default mode network in Alzheimer's disease: an fMRI study. *Neuroscience Letters, 578*, 171–175. doi:10.1016/j.neulet.2014.06.043.